Reac Kinet Mech Cat (2014) 112:101–116
DOI 10.1007/s11144-014-0677-3

The beneficial use of ultrasound irradiation and nitrate/acetate metal precursors in the co-precipitation synthesis and characterization of nanostructured $CuO–ZnO–Al_2O_3$ catalyst for methanol synthesis

Somaiyeh Allahyari · Mohammad Haghighi · Amanollah Ebadi · Shahin Hosseinzadeh · Habib Gavam Saeedi

Received: 31 October 2013 / Accepted: 18 January 2014 / Published online: 11 February 2014

Abstract A $CuO–ZnO–Al_2O_3$ catalyst was synthesized by an ultrasound assisted co-precipitation method and compared with the one synthesized by a conventional co-precipitation method. The characterization results of XRD, BET, FESEM and FTIR indicated that the physicochemical properties of the catalysts are strongly influenced by the formulated precursor and the synthesis method. The morphology of the catalyst precipitated under ultrasound irradiation was well-defined and agglomoration-free with average size particle of 32.3 nm. The dispersion of CuO and the surface area of the catalyst exhibited an improvement in acetate based catalyst. The high degree of synergism effect between CuO and other components in $CuO–ZnO–Al_2O_3$ catalyst was expected in the acetate-based catalyst synthesized with ultrasound assisted co-precipitation method due to low crystallinity and small size of copper species. The catalytic performance for the synthesis of methanol was examined at 200–300 °C and 10–40 bar in a stainless steel reactor. The $CuO–ZnO–Al_2O_3$ catalyst synthesized from acetate precursor precipitated under ultrasound irradiation exhibited a supreme catalytic activity at 275 °C, 40 bar, 18,000 cm^3/g h and $H_2/CO = 2$ in terms of CO conversion and methanol yield.

Keywords $CuO–ZnO–Al_2O_3$ · Methanol synthesis · Ultrasound · Co-precipitation

S. Allahyari · M. Haghighi · A. Ebadi · S. Hosseinzadeh · H. Gavam Saeedi
Chemical Engineering Faculty, Sahand University of Technology, P.O. Box 51335-1996, Sahand New Town, Tabriz, Iran

S. Allahyari · M. Haghighi (✉) · A. Ebadi · S. Hosseinzadeh · H. Gavam Saeedi
Reactor and Catalysis Research Center (RCRC), Sahand University of Technology, P.O. Box 51335-1996, Sahand New Town, Tabriz, Iran
e-mail: haghighi@sut.ac.ir
URL: http://rcrc.sut.ac.ir

Introduction

The methanol synthesis using copper-containing catalysts has received considerable attention in recent years, because of the importance of methanol as a common chemical feedstock for several important chemicals and also methanol as a potential alternative energy to fossil fuels [1, 2]. The main reactions involved in the formation of methanol from syngas are the methanol synthesis from CO and CO_2 and water gas shift (WGS) reactions [3, 4]:

$$CO + 2H_2 \leftrightarrow CH_3OH \qquad \Delta H^{o}_{298} = -90.8 \text{ kJ/mol}$$

$$CO + 2H_2O \leftrightarrow CO_2 + 2H_2 \qquad \Delta H^{o}_{298} = -41.0 \text{ kJ/mol}$$

$$CO_2 + 3H_2 \leftrightarrow CH_3OH + H_2O \qquad \Delta H^{o}_{298} = -49.4 \text{ kJ/mol}$$

Although new catalysts such as noble metal doped copper based catalysts have been recently investigated for methanol synthesis [5, 6], common $Cu/ZnO/Al_2O_3$ based catalysts are employed in wide range of methanol synthesis processes [7–10]. The advantages of the CuO/ZnO systems include low cost and high selectivity to methanol, and the system is mature and well-developed [11]. To date, the best catalytic performance has been achieved over $Cu/ZnO/Al_2O_3$ catalysts prepared by the co-precipitation method [8, 12–14]. One of the major drawbacks of this method is the inability to control the size of the precipitating particles and their subsequent aggregation [15]. $Cu–ZnO–Al_2O_3$ catalysts also were prepared by supercritical fluid drying, vacuum freeze-drying, flame combustion synthesis, microwave irradiation and organic complex decomposing [16–18]. Hybrid methods in which de-agglomeration of the synthesized nano-material control the size of particles should be considered. The precipitated gel experiences ultra-high shear forces and cavitational heating under ultrasound irradiation which leads to the formation of nano-phase particles and high-phase purity in complex metal oxides. Moreover, in liquids irradiated with ultrasound, acoustic cavitation drives bubble collapse producing intense local heating, high pressures, and very short lifetimes; these transient, localized hot spots facilitate chemical reactions [19–24] during synthesis which can enhance and promote nucleation rate and dispersion of the fine active metal particles on the carrier. To the best of our knowledge, there is no extensive study for the application of ultrasound during co-precipitation of $CuO–ZnO–Al_2O_3$ catalyst. Bearing the afore-mentioned aspects, the present investigation is focused on understanding the influence of ultrasound irradiation on properties of co-precipitated $CuO–ZnO–Al_2O_3$ catalyst with different precursors of copper and zinc. The characterization of the catalyst was carried out using various methods such as nitrogen adsorption Brunauer–Emmett–Teller analysis (BET), X-ray diffraction (XRD), Fourier-transformed infrared (FTIR) and field emission scanning electron microscopy (FESEM). Additionally, the influences of ultrasound irradiation and type of precursor on the performance of the synthesized catalysts were investigated.

Materials and methods

Materials

Copper(II) nitrate ($Cu(NO_3)_2{\cdot}3H_2O$), copper(II) acetate ($((CH_3COO)_2Cu{\cdot}H_2O$), zinc(II) nitrate ($Zn(NO_3)_2{\cdot}3H_2O$), zinc acetate ($((CH_3COO)_2Zn{\cdot}2H_2O$), aluminum(III) nitrate ($Al(NO_3)_3{\cdot}9H_2O$) and ammonium carbonate ($(NH_4)_2CO_3$), were supplied by Merck, Germany. All of the materials were used as received without any further purification. H_2, argon and CO were all of high purity and were purchased from Technical Gas Services in Ajman, UAE.

Nanocatalysts preparation and procedures

$Cu/ZnO/Al_2O_3$ (CZA) was used as the methanol synthesis catalyst. A 1.0 M solution containing the appropriate weight ratios of metal salts with atomic ratio of Cu:Zn:Al = 6:3:1 was prepared. This solution and a 1.0 M aqueous solution of ammonium carbonate were simultaneously added into the baker at the pH range of 7–8 and temperature of 70–80 °C under irradiation of ultrasound. Sonication was carried out on a SONOPULS HD 3200. The slurry irradiated with a high-intensity ultrasonic employing a direct immersion titanium horn of 1 cm^2 (20 kHz, power output 150 W/cm^2) which was inserted 1 cm below the solution, under a flow of argon for 60 min. The resulting precipitates were dried at 110 °C for 12 h after filtration and washing, and then calcined at 350 °C for 5 h.

Boehmite (3 wt%) was used for shaping the catalysts. The diameter of the pellets was 5 mm and the height was 5 mm. After shaping, the pellets dried at 110 °C and calcined at 350 °C for 5 h. In this paper, the CZA catalyst synthesized from acetate and nitrate precursors was named as CZA-A and CZA-N, respectively. P and U after the name of catalyst was referred to synthesis method: P for co-precipitation CZA and U for ultrasound assisted co-precipitation of CZA.

Nanocatalysts characterizations

XRD analysis was performed on Siemens diffractometer D5000 with a Cu Kα radiation source operating at 40 kV and 30 mA in a scanning range of $2\theta = 5°–70°$. The diffraction peaks of the crystalline phase were compared with those of standard compounds reported in the Joint Committee of Powder Diffraction Standards (JCPDS) database files. The microstructure and morphology were studied by FESEM (HITACHI S-109 4160). The specific surface areas of the samples were determined by BET method on Quantachorom CHEMBET-3000 apparatus. FTIR of the powders was recorded on UNICAM 4600 Fourier spectrometer in a range of 4,000–400 cm^{-1} by the KBr pellet method.

Nanocatalyst performance test toward syngas to methanol

The catalytic activity was evaluated in a fixed bed reactor made of stainless steel with an inner diameter of 5 mm with 0.2 g of catalyst. The experimental setup is

shown schematically in Fig. 1. A K-type thermocouple was inserted into the catalyst bed to detect the temperature of reaction along the axial length of the reactor. The reactor was set inside a conventional furnace. The exit line from the reactor to the gas-sampling valve in GC was heated to prevent condensation of any volatile products. Prior to the reaction, the catalyst was reduced by hydrogen under atmospheric pressure at 275 °C for 3 h. After reduction, the synthesis gas was fed into the reactor. Experiments were performed at temperatures ranging from 200 to 300 °C and pressures ranging from 10 to 40 bar. A mixture of carbon monoxide and hydrogen (feed) at a H_2/CO ratio of 2 was supplied through mass flow controllers (Beijing Sevenstar Electronics Co., Ltd.) to a pre-heater at 120 °C, then to the catalyst bed at the designated reaction temperature. Compositions of feed and reactor effluent gas were monitored by a gas chromatograph (GC Chrom, Teif Gostar Faraz, Iran) equipped with two electrical controlled six-port switching valves, a 1 ml sample loop, a flame ionization detector (FID) and a thermal conductivity detector (TCD). The GC column was packed with a HP plot-U column (Agilent) was used for the separation of methanol and CO_2, and a molecular sieve 5A column (Agilent) was used for separation of H_2, N_2, CH_4 and CO. The effect of the operating variables such as reaction temperature, pressure and GHSV on the catalytic performance of the CZA nanocatalysts was investigated to identify effect of metal precursor and ultrasound irradiation during co-precipitation for synthesis of the most active catalyst for methanol synthesis process.

Results and discussion

Effect of precursor and synthesis method on CZA properties

XRD analysis

Fig. 2 shows the XRD patterns of CZA catalysts with different precursors synthesized by co-precipitation and ultrasound assisted co-precipitation methods. CuO peaks are observed in all four catalysts with different metal precursors and synthesis methods. No clear ZnO peaks are detectable. It seems CuO and ZnO peaks are not finely resolved. It is found that the phase crystalline of the CuO markedly depends on the type of synthesis method. CuO peaks are broader and consequently more highly dispersed in ultrasound-assisted co-precipitated catalysts. The broad reflections in these catalysts indicate that part of Cu may be dissolved in the Zn matrix or the CuO phase is in intimate contact with the ZnO phase [25]. This result also reveals that the particles size of CuO and ZnO are much smaller in the sonochemical synthesis method and the copper and zinc exhibit amorphous-like or less ordered structural features [26]. According to the Scherrer's equation, the CuO crystallite sizes in ultrasound assisted co-precipitated catalysts were almost similar; 5.6 and 5.8 nm for CZA-NP and CZA-AP, respectively. In non-sonicated catalysts, larger crystallites of CuO were found which consequently influences the dispersion of the CuO active phase. CuO crystallite sizes were 6.4 and 6.9 nm for CZA-AP and CZA-NP, respectively. Acetate based catalyst showed smaller CuO crystallites.

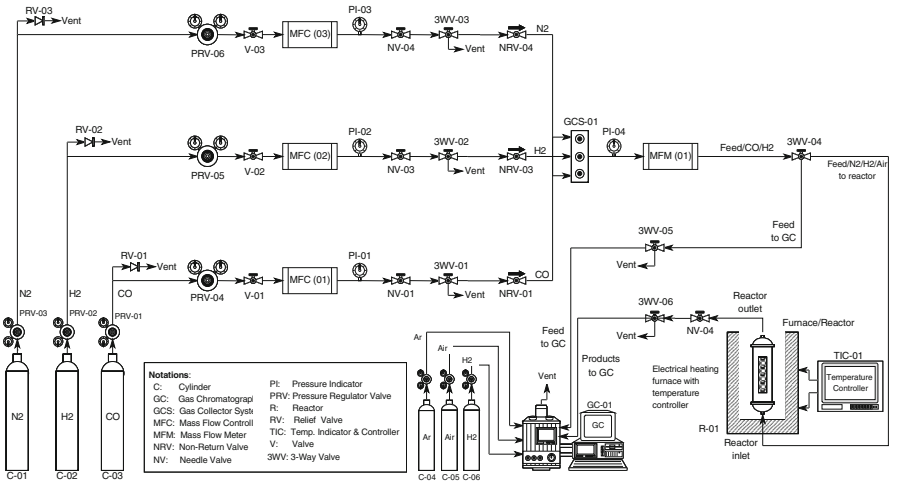

Fig. 1 Experimental setup for testing of catalytic performance of CZA nanocatalyst toward conversion of syngas to methanol

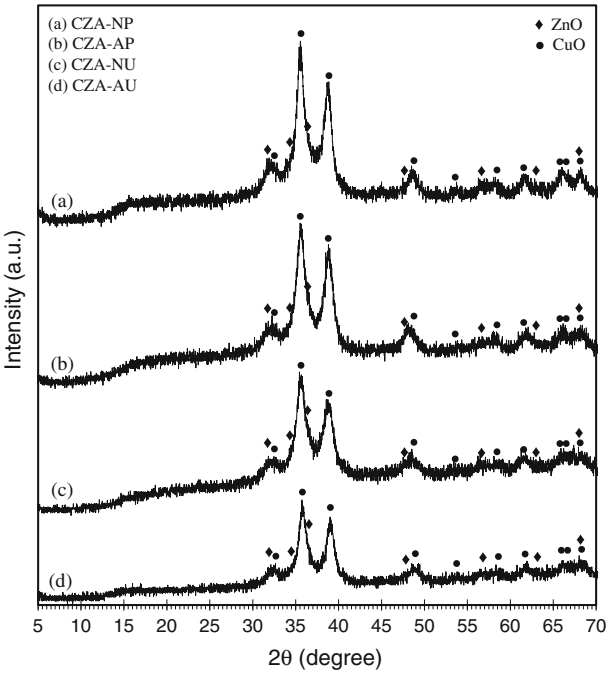

Fig. 2 XRD patterns of synthesized CZA using different precursors and methods: *a* CZA-AP, *b* CZA-AU, *c* CZA-NP and *d* CZA-NU

Reflections due to Al_2O_3 could not be observed in the both catalysts form. This is due to the fact that Al_2O_3 is present in small quantities and may be in the amorphous state or might be due to low calcination temperature, i.e. 350 °C at which formation

of this metal oxide crystalline species is improbable. This observation is in good agreement with previous studies [27, 28]. There are controversies concerning the role of ZnO, ranging from spill over model to morphology effect to active site model [29]. High crystallinity of CuO or ZnO means that these materials form their crystals independently without any interaction between them. Therefore, in the highly crystalline CZA catalyst, the interaction between Cu and Zn and consequently their synergetic effect will be weak. According to the XRD patterns of CZA-NP, CZA-NU, CZA-AU and CZA-AP catalysts, we expect higher reactivity of ultrasound assisted co-precipitated catalyst in methanol synthesis due to the low crystallinity of components and hence higher dispersion of metals and stronger interaction between CuO and ZnO. No diffraction peaks ascribed to $ZnAl_2O_4$ or $CuAl_2O_4$ spinel-like structures were detected, which was probably due to the moderate calcination conditions used.

FESEM analysis

FESEM micrographs of the CZA-AU, CZA-NU, CZA-AP and CZA-NP samples in Fig. 3 reveal that the particles are of uniform shape almost spherical in all the samples but the particles size are different. Ultrasound assisted co-precipitated (CZA-U) samples independent of the precursor type showed more uniform morphology with smaller particle size. This observation confirms high and homogenous nucleation and limited particle growth during ultrasound irradiation. In the CZA-AU catalyst, unlike in CZA-NP, CZA-NU and CZA-AP, no agglomeration of particles has been observed. The CZA-AU particles lost their spherical shape and smooth surface in other catalysts has been vanished. Individual particles with rough surface and sharp corners can be observed in this catalyst, which confirms the presence of defects and structural disorder in the catalyst in good agreement with XRD results. The compact morphology disappeared in the CZA-AU catalyst because of the synthesis method and precursor type. Fig. 4 shows the size distribution histogram of the CZA catalyst synthesized with different methods and different precursors. The CZA-AU catalyst has minimum size of 15.9 nm. The maximum size of particles in the CZA-AU nanocatalyst was 66.5 nm and the average particle size was 32.3 nm. The major part of particles is in the range of 20–30 nm. The worst results were attributed to CZA-NP catalyst with average, minimum and maximum size of 48.3, 25.3 and 99.9 nm. The order of average particle size can be arranged in this order: CZA-AU < CZA-NU < CZA-AP < CZA-NP.

Although FESEM micrographs indicate the particle size and XRD patterns reveal crystallite sizes, which are independent concepts, but the trend observed in XRD was almost repeated in FESEM as well.

BET analysis

The specific surface area of the CZA catalysts with different precursors and synthesis methods has been illustrated in Fig. 5. Ultrasound irradiation results in the formation of small and well-dispersed particles, which lead to a higher surface area

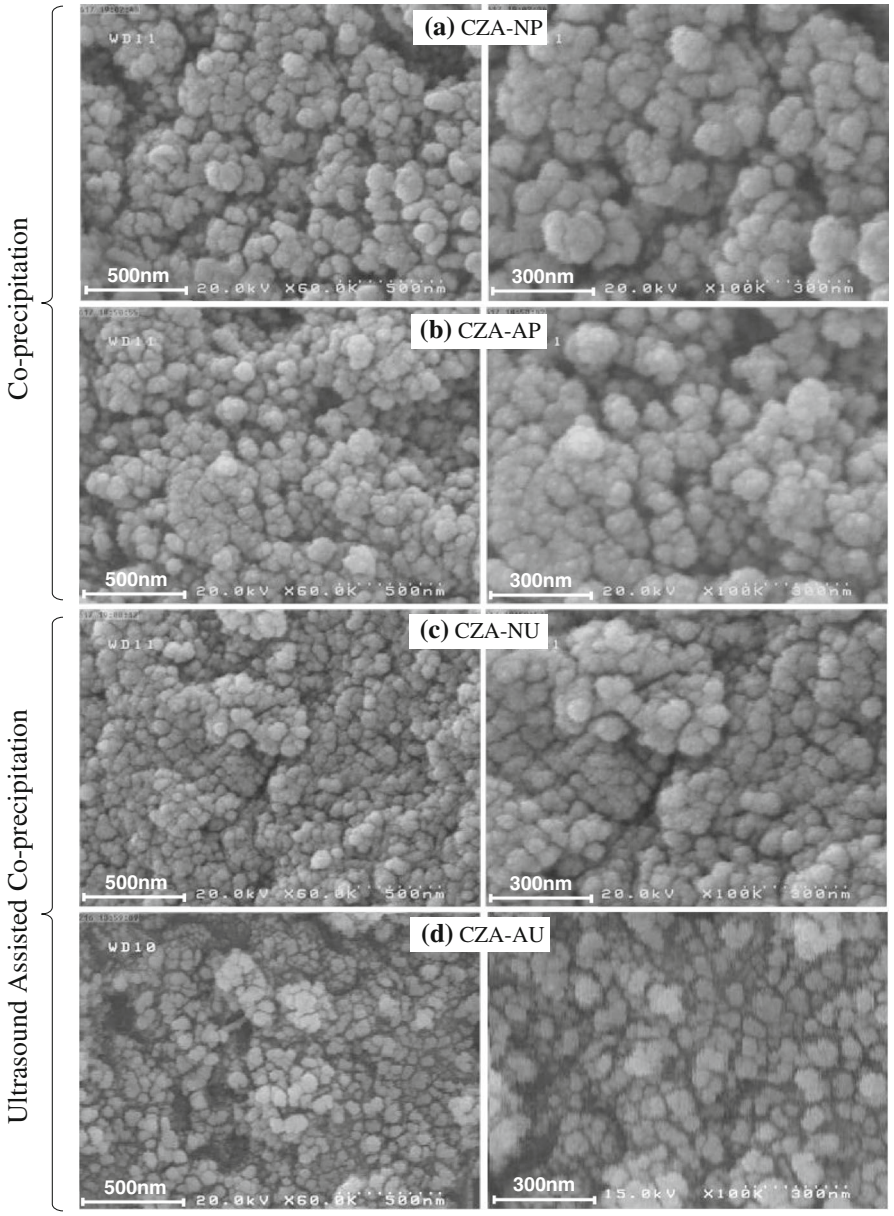

Fig. 3 FESEM images of synthesized CZA using different precursors and methods: **a** CZA-NP, **b** CZA-AP, **c** CZA-NU and **d** CZA-AU

of ultrasound irradiated catalysts. Acetate precursors have higher surface area in similar samples compared to nitrate based catalysts. The lower vapor pressure of acetates leads to a higher nucleation rate that produces smaller and more dispersed particles which result in higher surface area for acetate based catalysts. Moreover,

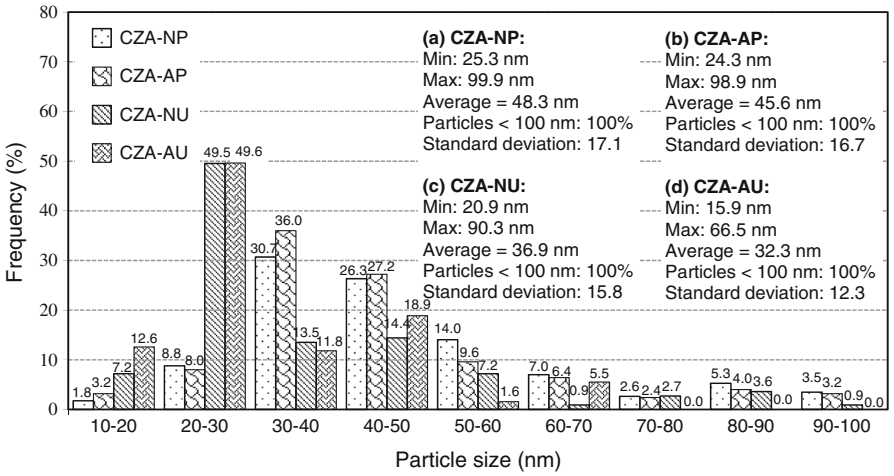

Fig. 4 Surface size distribution histogram of synthesized CZA using different precursors and methods

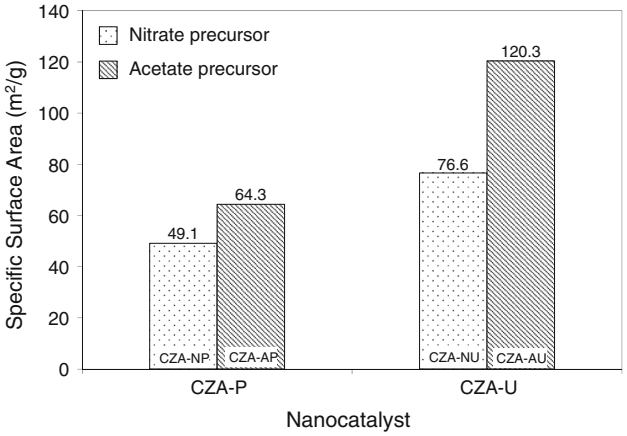

Fig. 5 BET surface area of synthesized CZA using different precursors and methods

the sonochemical synthesis of a volatile precursor occurs in cavity region in which the cooling rate is high. Therefore, the crystallinity of metal oxide formulated from the acetate precursor will be low (as evidenced by XRD) and higher surface area will be observed.

FTIR analysis

Fig. 6 shows the FTIR spectra of synthesized CZA nanocatalysts via the co-precipitation and ultrasound assisted co-precipitation method with different precursors. The bending around 512 cm^{-1} is the signature of ZnO [30, 31];

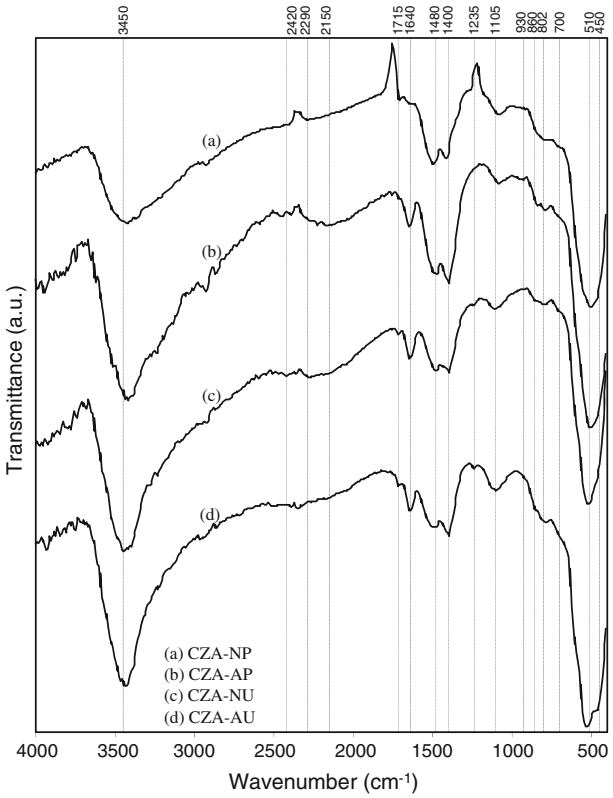

Fig. 6 FTIR spectra of synthesized CZA using different precursors and methods: *a* CZA-NP, *b* CZA-AP, *c* CZA-NU and *d* CZA-AU

O–Cu–O bonding causes bending close to 500 and 1,384 cm^{-1} [32] and the bending near 582 cm^{-1} is identified to be the characteristic of Al_2O_3 [33]. The broad absorption bands at 3,450 cm^{-1} are attributed to the hydroxyl groups, which are extensively hydrogen bonded. The band at ca. 1,645 cm^{-1} is assigned to the bonding vibration mode of the interlayer water molecules [34–37]. Furthermore, no characteristic bond was observed for other impurities such as $Cu(OH)_2$ or $Zn(OH)_2$ in the FTIR patterns. These results support and complement the XRD data. The peak at 2,370 cm^{-1} is associated with the C–H stretching mode of atmospheric hydrocarbons on the surface of the catalysts [38]. The bands at 1,490 cm^{-1} are corresponding to C=O and C=C groups [39].

Catalytic performance of CZA toward syngas to methanol

Effect of precursor

The CO conversion and methanol yield as a function of temperature is presented in Table 1 using CZA catalysts formulated from two different precursors: acetate

based and nitrate based catalysts. The temperature was increased at an interval of 25 from 200 to 300 °C. As shown in Table 1, when the reaction temperature increased from 200 to 275 °C, the CO conversion increased gradually for both precursors. A further increase in reaction temperature to 300 °C decreased the CO conversion. The existence of optimum is partly due to the declining equilibrium value of CO conversion with temperature increasing. It was observed that the catalytic activity of the acetate-based catalyst was higher than the activity of the nitrate-based catalyst almost at all temperature ranges on the basis of our experimental results. Kim et al. [40] confirmed the catalysts formulated from the acetate-based precursors show better activity in conversion of CO rather than nitrate based catalysts. The reason caused the difference of reactivity between CZA-A and CZA-N was related to XRD, FESEM and BET results. It seems the crystallinities of CuO, surface area and overall morphology of the catalyst would exert an influence on the reactivity of catalyst. The higher crystallinity of CuO in nitrate based catalyst indicates the independency of crystals, lower interaction between them and less degree of synergism. Therefore, the lower reactivity is expected at the higher crystallinity as observed for nitrate based catalysts.

According to Table 1, the extent of methanol yield over CZA-AU was higher than that of CZA-NU. With increasing temperature, a maximum in methanol yield was observed at 275 °C. At temperatures higher than 275 °C, the methanol yield decreased. Interestingly, the highest methanol yield is accompanied by the highest CO conversion on these catalysts. According to the results, it is clear that acetate based catalysts demonstrates excellent catalytic performance in terms of product yield as well. These results are in good agreement with FESEM; BET and XRD analyses that showed acetate based catalysts have more uniform morphology, higher surface area, higher interaction and dispersion. It appears that the feed conversion and product yield are proportional to catalyst surface area and crystallinity of the CZA catalysts, which are dependent on the formulated precursors. Two important regions in sonochemistry reactions are inside the cavity and interfacial region, which surrounds the collapsing bubble. While the implosive collapse raises the local temperature to 5,000 K and the pressures to a few hundred atmospheres in first region, the temperature reached after collapse 1,900 K in the second region [19]. The sonochemical synthesis of volatile precursors like acetates occurs in the first

Table 1 Effect of precursor (metal nitrate/acetate) on CO conversion and methanol yield over nano-structured CuO–ZnO–Al_2O_3 catalyst at different temperatures

Run	T (°C)	P (bar)	(cm^3/g h)	H_2/CO	CO conversion		Methanol yield	
					CZA-NU	CZA-AU	CZA-NU	CZA-AU
1	200	40	18,000	2	2.6	5.07	2.12	4.96
2	225	40	18,000	2	2.97	7.06	2.45	6.63
3	250	40	18,000	2	7	7.78	5.74	7.78
4	275	40	18,000	2	9.62	10.14	6.37	9.1
5	300	40	18,000	2	8.19	6.77	5.5	5.37

region, but sonochemical reactions of non-volatile compounds occur in the area closer to the second region. The synthesis of catalyst particles in the high temperature region cause higher cooling rates, which creates CZA particles with lower crystallinity and hence higher interaction. The strong interaction between CuO and ZnO improves the synergism effect in CO conversion over CuO and hydrogenation over ZnO according to the mechanism of methanol synthesis and increases the reactivity of the catalyst.

Effect of synthesis method

Figs. 7 and 8 indicate the effect of pressure on catalytic reactivity in terms of CO conversion and methanol yield with co-precipitated and ultrasound assisted co-precipitated CZA catalysts. The CO conversion increased with pressure for all CZA catalysts. According to thermodynamics, pressure has a positive effect on the methanol synthesis. The synthesis of methanol reaction caused the decrease in volume; the reactivity was enhanced as the pressure was increased. The sonochemicaly synthesized CZA catalyst exhibited better reactivity in terms of CO conversion and methanol yield at all pressure ranges compared with co-precipitated CZA catalyst. In liquids irradiated with ultrasound, acoustic cavitation drives bubble collapse producing intense local heating, high pressures and very short life times. These transient, localized hot spots facilitate chemical reactions [19–24, 40] during synthesis which can enhance and promote nucleation rate and dispersion of the fine active metal particles on the support. Acoustic cavitation can induce extraordinary local heating and can provide enormous cooling rates ($>10^9$ K/s), which produces amorphous metal powders using the sonochemical decomposition of volatile organometallics. The sonochemically synthesized amorphous powders may have important catalytic applications, especially due to very high surface areas and nanometer cluster size.

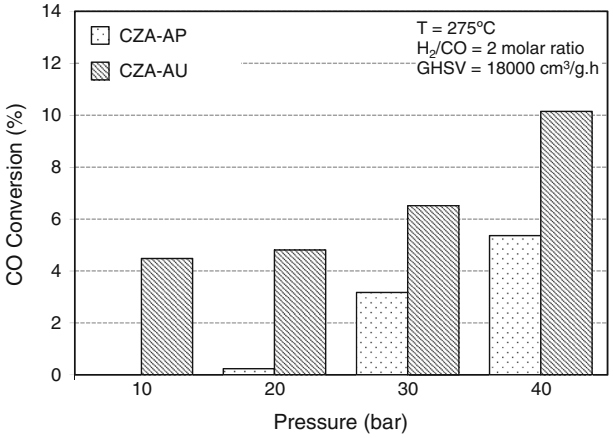

Fig. 7 Effect of the synthesis method on the CO conversion over the nanostructured CuO–ZnO–Al_2O_3 catalyst at different pressures

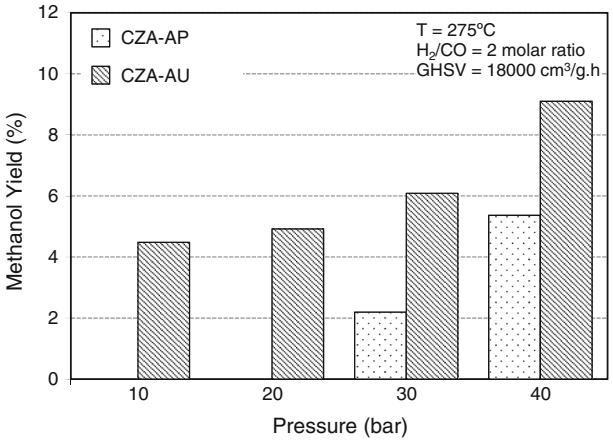

Fig. 8 Effect of the synthesis method on the methanol yield over the nanostructured CuO–ZnO–Al_2O_3 catalyst at different pressures

Table 2 Different copper based catalysts evaluated in CO hydrogenation to synthesis of methanol

Catalyst	Synthesis method	T (°C)	P (bar)	X_{CO} (%)	S_{CH3OH} (%)	Ref.
Cu/ZrO_2	Co-precipitation	250	30	1.73	94.2	[41]
Cu/ZrO_2	Co-precipitation	260	60	8.7	82	[42]
Cu/ZrO_2	Alco-gel	260	60	12.7	86	[42]
Cu/ZnO/ZrO_2	Co-precipitation	250	34	7	15	[43]
CuO/ZnO/ Al_2O_3	Ultrasound co-precipitation	275	40	10.1	90	This work

The selectivity in all pressure ranges were in the range of 90–100 %. Small amounts of CO_2 and DME are side products and no methane and ethanol was detected. So the methanol yield followed the CO conversion trend. Increasing pressure enhanced the methanol yield and ultrasound assisted catalysts showed better reactivity in producing methanol.

Table 2 illustrates different copper based catalysts evaluated in CO hydrogenation to synthesize methanol. CO conversion and methanol selectivity are criteria to compare the results obtained to that of investigated in literature to ascertain the effect of ultrasound irradiations during precipitation. Pokrovski et al. [41] revealed that the substitution of Ce for Zr into the ZrO_2 lattice results in significantly enhanced methanol synthesis activity. Their synthesis method was co-precipitation and the CO conversion increased from 1.73 % in the case of Cu/ZrO_2 to 5.30 % in the case of Cu/$Ce_{0.3}Zr_{0.7}O_2$ catalyst.

Bai et al. [42] examined two different synthesis methods and founded CO conversion increased from 8.7 to 12.7 % with changing the synthesis method from co-precipitation to the alcogel/thermal treated with nitrogen method. The selectivity of methanol also changed from 82 to 86 %. In the work of Suh et al. [43], the Cu/

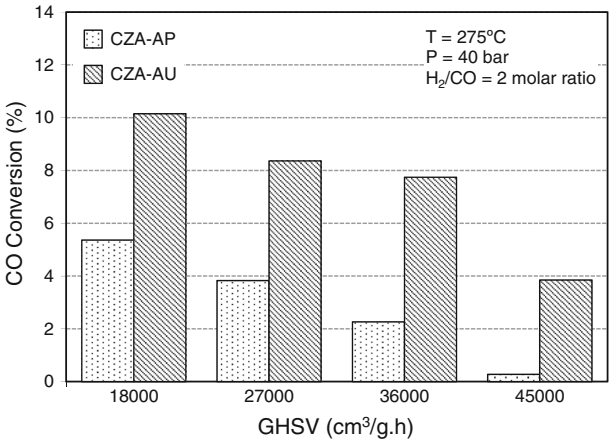

Fig. 9 Effect of the synthesis method on the CO conversion over the nanostructured CuO–ZnO–Al_2O_3 catalyst at different GHSVs

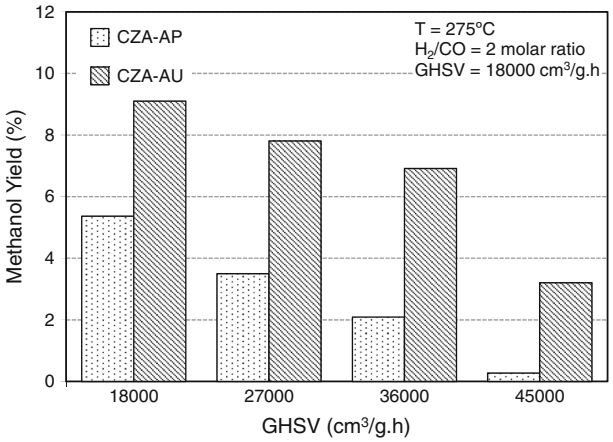

Fig. 10 Effect of the synthesis method on the methanol yield over the nanostructured CuO–ZnO–Al_2O_3 catalyst at different GHSVs

ZnO/ZrO_2 catalysts with 5 wt% ZrO_2 showed 7 % CO conversion. With increasing ZrO_2 content, CO conversion increased and in 35 wt% ZrO_2, the CO conversion descends to 10 %. Comparing results with the literature shows that the CZA catalyst synthesized with the ultrasound assisted co-precipitation method has simultaneously highly desirable product selectivity and also high feed conversion.

The effect of GHSV on the CO conversion and the methanol yields with the differently synthesized CZA catalysts was studied and the results are presented in Fig. 9. As shown, a progressive decrease in the conversion of CO was observed with an increase in the space velocity, especially from 36,000 to 45,000 cm^3/g h. When the space velocity was increased from 36,000 to 45,000 cm^3/g h, the CO conversion

was decreased significantly from 7.7 to ca. 3.8 % for the sonochemically synthesized CZA catalyst and from 2.2 to ca 0 % for the co-precipitated catalyst. Higher space velocity means shorter reaction time, which accounts for the lower conversion of syngas. The effect of GHSV on methanol yield is illustrated in Fig. 10. Increasing GHSV decreased methanol yield from 9.1 to 3.2 % for the CZA-AU catalyst. The selectivity of methanol (not shown) even at high GHSVs is high for these catalysts but due to less amount of syngas conversion, methanol yield follows up the previous trend for CO conversion. From Figs. 9 and 10, it can be concluded that ultrasound assisted synthesized CZA catalyst shows better activity in all GHSV ranges than that of co-precipitated CZA catalyst.

Conclusions

The ultrasound method offers several advantages over the conventional precipitation routes, such as well-defined structure, small CuO crystals, high CuO dispersion, high interaction and high BET surface area. Moreover, the investigation about precursors showed better physiochemical properties of acetate formulated CZA catalyst compared with nitrate based catalyst. We evaluated the activity of investigated methanol synthesis catalysts in a stainless steel fixed bed reactor at 200–300 °C and 10–40 bar. The acetate based catalysts precipitated under ultrasound irradiations exhibited excellent CO conversion and methanol yield; 10.1 % CO conversion and 9.1 % methanol yield was found at 275 °C and 40 bar for CZA-AU catalyst.

Acknowledgments The authors gratefully acknowledge Sahand University of Technology for the financial support of the project as well as Iran Nanotechnology Initiative Council for complementary financial support.

References

1. Raudaskoski R, Turpeinen E, Lenkkeri R, Pongrácz E, Keiski RL (2009) Catalytic activation of CO_2: use of secondary CO_2 for the production of synthesis gas and for methanol synthesis over copper-based zirconia-containing catalysts. Catal Today 144(3–4):318–323
2. Wang F, Liu Y, Gan Y, Ding W, Fang W, Yang Y (2013) Study on the modification of Cu-based catalysts with cupric silicate for methanol synthesis from synthesis gas. Fuel Process Technol 110:190–196
3. Phan XK, Bakhtiary-Davijany H, Myrstad R, Pfeifer P, Venvik HJ, Holmen A (2011) Preparation and performance of Cu-based monoliths for methanol synthesis. Appl Catal A 405(1–2):1–7
4. Karelovic A, Bargibant A, Fernández C, Ruiz P (2012) Effect of the structural and morphological properties of Cu/ZnO catalysts prepared by citrate method on their activity toward methanol synthesis from CO_2 and H_2 under mild reaction conditions. Catal Today 197(1):109–118
5. Mierczynski P, Kaczorowski P, Maniecki TP, Bawolak-Olczak K, Maniukiewicz W (2013) The influence of Pd loading on the physicochemical properties of the Cu–Cr–Al methanol synthesis catalysts. React Kinet Mech Cat 109:13–27
6. Mierczynski P, Maniecki TP, Maniukiewicz W, Jozwiak WK (2011) $Cu/Cr_2O_3{\cdot}3Al_2O_3$ and $Au–Cu/Cr_2O_3{\cdot}3Al_2O_3$ catalysts for methanol synthesis and water gas shiftreactions. React Kinet Mech Cat 104:139–148

7. Khoshbin R, Haghighi M, Asgari N (2013) Direct synthesis of dimethyl ether on the admixed nanocatalysts of CuO–ZnO–Al_2O_3 and HNO_3-modified clinoptilolite at high pressures: surface properties and catalytic performance. Mater Res Bull 48(2):767–777
8. Khoshbin R, Haghighi M (2013) Direct syngas to DME as a clean fuel: the beneficial use of ultrasound for the preparation of CuO–ZnO–Al_2O_3/HZSM-5 nanocatalyst. Chem Eng Res Des 91(6):1111–1122
9. Khoshbin R, Haghighi M (2013) Preparation and catalytic performance of CuO–ZnO–Al_2O_3/clinoptilolite nanocatalyst for single-step synthesis of dimethyl ether from syngas as a green fuel. J Nanosci Nanotechnol 13(7):4996–5003
10. Khoshbin R, Haghighi M (2012) Urea-nitrate combustion synthesis and physicochemical characterization of CuO–ZnO–Al_2O_3 nanoparticles over HZSM-5. Chin J Inorg Chem 28(9):1967–1978
11. Chinchen GC, Denny PJ, Jennings JR, Spencer MS, Waugh KC (1988) Synthesis of methanol: part 1. Catal Kinet Appl Catal 36:1–65
12. Saedy S, Haghighi M, Amirkhosrow M (2012) Hydrothermal synthesis and physicochemical characterization of CuO/ZnO/Al_2O_3 nanopowder. Part I: effect of crystallization time. Particuology 10(6):729–736
13. Chu Z, Chen H, Yu Y, Wang Q, Fang D (2013) Surfactant-assisted preparation of Cu/ZnO/Al_2O_3 catalyst for methanol synthesis from syngas. J Mol Catal A Chem 366:48–53
14. Budiman A, Ridwan M, Kim SM, Choi J-W, Yoon CW, Ha J-M, Suh DJ, Suh Y-W (2013) Design and preparation of high-surface-area Cu/ZnO/Al_2O_3 catalysts using a modified co-precipitation method for the water–gas shift reaction. Appl Catal A 462–463:220–226
15. Prasad K, Pinjari DV, Pandit AB, Mhaske ST (2011) Synthesis of zirconium dioxide by ultrasound assisted precipitation: effect of calcination temperature. Ultrason Sonochem 18(5):1128–1137
16. Jensen JR, Johannessen T, Wedel S, Livbjerg H (2003) A study of Cu/ZnO/Al_2O_3 methanol catalysts prepared by flame combustion synthesis. J Catal 218(1):67–77
17. Li Z, Yan S, Fan H (2013) Enhancement of stability and activity of Cu/ZnO/Al_2O_3 catalysts by microwave irradiation for liquid phase methanol synthesis. Fuel 106:178–186
18. Ning W, Shen H, Liu H (2001) Study of the effect of preparation method on CuO–ZnO–Al_2O_3 catalyst. Appl Catal A 211(2):153–157
19. Suslick KS, Price GJ (1999) Applications of ultrasound to materials chemistry. Annu Rev Mater Sci 29:295
20. Suslick KS, Hyeon T, Fang M, Cichowlas AA, William RM (1996) Chapter 8—sonochemical preparation of nanostructured catalysts. Advanced catalysts and nanostructured materials. Academic Press, San Diego, pp 197–212
21. Suslick KS, Hyeon T, Fang M, Cichowlas AA (1995) Sonochemical synthesis of nanostructured catalysts. Mater Sci Eng A 204(1–2):186–192
22. Suslick KS, McCleverty JA, Meyer TJ (2003) Sonochemistry. In: Comprehensive coordination chemistry II, Pergamon, Oxford, pp 731–739
23. Suslick KS, Robert AM (2003) In: Encyclopedia of physical science and technology. Sonoluminescence and sonochemistry, 3rd edn. Academic Press, New York, pp 363–376
24. Aguayo AT, Erena J, Sierra I, Olazar M, Bilbao J (2005) Deactivation and regeneration of hybrid catalysts in the single-step synthesis of dimethyl ether from syngas and CO_2. Catal Today 106(1–4):265–270
25. Robinson WRAM, Mol JC (1993) Temperature-programmed desorption study on supported copper-containing methanol synthesis catalysts. Appl Catal A 98(1):81–97
26. Jun K-W, Shen W-J, Rama Rao KS, Lee K-W (1998) Residual sodium effect on the catalytic activity of Cu/ZnO/Al_2O_3 in methanol synthesis from CO_2 hydrogenation. Appl Catal A 174(1–2):231–238
27. Venugopal A, Palgunadi J, Deog JK, Joo O-S, Shin C-H (2009) Dimethyl ether synthesis on the admixed catalysts of Cu–Zn–Al–M (M = Ga, La, Y, Zr) and gamma-Al_2O_3: the role of modifier. J Mol Catal A Chem 302(1–2):20–27
28. Wang L, Fang D, Huang X, Zhang S, Qi Y, Liu Z (2006) Influence of reaction conditions on methanol synthesis and WGS reaction in the syngas-to-DME process. J Nat Gas Chem 15(1):38–44
29. Sun K, Lu W, Qiu F, Liu S, Xu X (2003) Direct synthesis of DME over bifunctional catalyst: surface properties and catalytic performance. Appl Catal A 252(2):243–249
30. Goswami N, Sharma DK (2010) Structural and optical properties of unannealed and annealed ZnO nanoparticles prepared by a chemical precipitation technique. Physica E 42(5):1675–1682

31. Lee YC, Yang CS, Huang HJ, Hu SY, Lee JW, Cheng CF, Huang CC, Tsai MK, Kuang HC (2010) Structural and optical properties of ZnO nanopowder prepared by microwave-assisted synthesis. J Lumin 130(10):1756–1759
32. Hung C-M (2009) Synthesis, characterization and performance of CuO/La_2O_3 composite catalyst for ammonia catalytic oxidation. Powder Technol 196(1):56–61
33. Djelloul A, Aida MS, Bougdira J (2010) Photoluminescence, FTIR and X-ray diffraction studies on undoped and Al-doped ZnO thin films grown on polycrystalline α-alumina substrates by ultrasonic spray pyrolysis. J Lumin 130(11):2113–2117
34. Chen L, Li L, Li G (2008) Synthesis of CuO nanorods and their catalytic activity in the thermal decomposition of ammonium perchlorate. J Alloys Compd 464(1–2):532–536
35. Aghamohammadi S, Haghighi M, Karimipour S (2013) A comparative synthesis and physico-chemical characterizations of Ni/Al_2O_3–MgO nanocatalyst via sequential impregnation and sol–gel methods used for CO_2 reforming of methane. J Nanosci Nanotechnol 13(7):4872–4882
36. Abbasi Z, Haghighi M, Fatehifar E, Rahemi N (2012) Comparative synthesis and physicochemical characterization of CeO2 nanopowder via redox reaction, precipitation and sol–gel methods used for total oxidation of toluene. Asia-Pac J Chem Eng 7(6):868–876
37. Khatamian M, Khandar AA, Haghighi M, Ghadiri M, Darbandi M (2010) Synthesis, characterization and acidic properties of nanopowder ZSM-5 type ferrisilicates in the Na^+/K^+ alkali system. Powder Technol 203(3):503–509
38. Anandan K, Rajendran V (2011) Morphological and size effects of NiO nanoparticles via solvo-thermal process and their optical properties. Mater Sci Semicond Process 14(1):43–47
39. Capek L, Dedecek J, Wichterlova B, Cider L, Jobson E, Tokarova V (2005) Cu–ZSM-5 zeolite highly active in reduction of NO with decane: effect of zeolite structural parameters on the catalyst performance. Appl Catal B 60(3–4):147–153
40. Kim EJ, Park NK, Han GB, Ryu SO, Lee TJ (2006) A reactivity test of Cu–Zn-based catalysts prepared with various precursors and precipitates for the direct synthesis of DME. Process Saf Environ Prot 84(6):469–475
41. Pokrovski KA, Bell AT (2006) Effect of dopants on the activity of $Cu/M_{0.3}Zr_{0.7}O_2$ (M = Ce, Mn, and Pr) for CO hydrogenation to methanol. J Catal 244(1):43–51
42. Bai Y, He D, Ge S, Liu H, Liu J, Huang W (2010) Influences of preparation methods of ZrO_2 support and treatment conditions of Cu/ZrO_2 catalysts on synthesis of methanol via CO hydrogenation. Catal Today 149(1–2):111–116
43. Suh Y-W, Moon S-H, Rhee H-K (2000) Active sites in $Cu/ZnO/ZrO_2$ catalysts for methanol synthesis from CO/H_2. Catal Today 63(2–4):447–452